

Anisotropy of spin relaxation in metals

Bernd Zimmermann, Phivos Mavropoulos,* Swantje Heers, Nguyen H. Long, Stefan Blügel, and Yuriy Mokrousov
*Peter Grünberg Institut and Institute for Advanced Simulation,
Forschungszentrum Jülich and JARA, 52425 Jülich, Germany*
(Dated: October 26, 2021)

The concept of anisotropy of spin relaxation in non-magnetic metals with respect to the spin direction of the injected electrons relative to the crystal orientation is introduced. The effect is related to an anisotropy of the Elliott-Yafet parameter, arising from a modulation of the decomposition of the spin-orbit Hamiltonian into spin-conserving and spin-flip terms as the spin quantization axis is varied. This anisotropy, reaching gigantic values for uniaxial transition-metals (e.g. 830% for hcp Hf) as density-functional calculations show, is related to extended “spin-flip hot areas” on the Fermi surface created by the proximity of extended sheets of the surface, or “spin-flip hot loops” at the Brillouin zone boundary, and has no theoretical upper limit. Possible ways of measuring the effect as well as consequences in application are briefly outlined.

PACS numbers: 72.25.Rb,72.25.Ba,76.30.Pk,75.76.+j

Spin-relaxation processes are of fundamental importance for the realization of spintronic devices, which aim at utilizing the electron spin degree of freedom for processing and transfer of information [1]. A non-equilibrium spin-distribution will generally equilibrate and the corresponding information will be lost on a timescale of the spin-relaxation time T_1 . The dominant spin-relaxation mechanism in structure- and bulk-inversion symmetric, non-magnetic metals is the Elliott-Yafet mechanism [2, 3], which is due to scattering of electrons at phonons or impurities. Owing to the presence of spin-orbit coupling (SOC) in a solid, such scattering events will flip the spin of an electron with a certain probability, which depends on both the wavefunctions of the ideal crystal and the scattering potential. An estimate of the ratio between momentum- and spin-relaxation time, T_p and T_1 , can be given in the diffusive regime in a first approximation by neglecting the form of the scattering potential. Within this *Elliott approximation* one obtains that $T_p/T_1 \approx 4b^2$, where b^2 is the *Elliott-Yafet (or spin-mixing) parameter*, which we define below and which, being a property of the ideal crystal only [2, 3], is related to the spin-orbit coupling strength in a material. Thus, b^2 has since long been accepted as a measure of spin relaxation, provided that some mechanism of momentum relaxation is present. However, what has not been analyzed so far on a theoretical basis is the anisotropy of b^2 , leading to a certain anisotropy of spin relaxation [4].

We put our notion of anisotropy in more precise terms by the following considerations. In an experiment measuring spin relaxation the injected electrons are always characterized by the axis of spin polarization which is determined e.g. by the external magnetic field in conduction-electron spin resonance or by the direction of magnetization of ferromagnetic leads in spin-injection or giant-magnetoresistance experiments. For our purposes we call this direction the *spin quantization axis* (SQA). As it turns out, the SQA relative to the crystal lattice matters for the value of b^2 , and not just by a little. This gives us the notion of anisotropy of the Elliott-Yafet parameter and consequently of spin relaxation: It will thus make a difference if spins are injected into a metal from a ferromag-

net whose magnetization is normal to the interface, compared to being parallel. Since the spin population decays exponentially with respect to the distance from the injection point, with T_1 entering in the exponent, the anisotropy can make a difference between e.g. a well-operating and a defective giant-magnetoresistance junction. One realizes also that we are faced with an anisotropy of an irreversible process, i.e., of the entropy production during relaxation. This can have far-reaching consequences, for example in the spin-entropy induced Peltier cooling in nanojunctions [7]. In this respect this anisotropy is fundamentally different from other, known SOC effects, such as the magnetocrystalline anisotropy energy of ferromagnets or the anisotropic magnetoresistance which arise from small changes of the band energies depending on the magnetization direction. From a band-structure point of view, in a nonmagnetic metal the choice of the SQA does not influence the band energies, but it manifests itself through matrix elements determining the orbital and spin character of the Bloch states. This, for example, leads to large changes of the spin Hall conductivity in non-cubic transition metals when the direction of the spin current’s polarization is varied [8]. One also expects an anisotropy in the spin susceptibility, since the spin-mixing parameter of a state is directly related to its response to a Zeemann field.

In this Letter, we investigate the anisotropy of the Elliott-Yafet parameter in metals. For this purpose we employ density functional theory, which has been successfully applied in the past to calculate the spin-mixing parameter in various metals [9, 10]. Our main finding is that in non-cubic transition metals, or generally metallic systems of lowered symmetry, e.g. in the hcp structure, the anisotropy of the Elliott-Yafet parameter can be gigantic. We also demonstrate that in metals with cubic symmetry, such as e.g. bcc tungsten or fcc gold, this anisotropy is much smaller, although it can still reach large values. Moreover, we analyze the Fermi surface properties of the spin-mixing anisotropy and provide simple arguments for a microscopic understanding of our results. Our choice of materials (*5d* metals) is based on their similar spin-orbit strength, but different crystal structures, which at the end

brings about anisotropy values differing by orders of magnitude.

The Elliott-Yafet theory is based on the observation that the spin-orbit coupling of the lattice ions causes the Bloch eigenstates to be a superposition of spin-up and spin-down character. This superposition is often called *spin mixing*. The spin-orbit Hamiltonian can be divided into a spin-conserving $\xi(LS)_{\parallel}$ and a spin-flip part $\xi(LS)^{\uparrow\downarrow}$, given respectively by the first and second parts of the r.h.s. of the following expression:

$$\xi \mathbf{L} \cdot \mathbf{S} = \xi L_{\hat{s}} S_{\hat{s}} + \frac{1}{2} \xi (L_{\hat{s}}^+ S_{\hat{s}}^- + L_{\hat{s}}^- S_{\hat{s}}^+). \quad (1)$$

Here, ξ is the spin-orbit coupling strength, \hat{s} is a unit vector in the direction of the spin- (and generally angular momentum-) quantization axis, \mathbf{L} and $\mathbf{S} = \frac{\hbar}{2} \boldsymbol{\sigma}$ are the orbital and spin angular momentum operators respectively, $L_{\hat{s}} = \mathbf{L} \cdot \hat{s}$, $S_{\hat{s}} = \mathbf{S} \cdot \hat{s}$, and $L_{\hat{s}}^{\pm}$ and $S_{\hat{s}}^{\pm}$ are the corresponding raising and lowering operators for angular momentum and spin in the reference frame specified by the direction vector \hat{s} (defining the SQA). It is clear that the dot product $\mathbf{L} \cdot \mathbf{S}$ is independent of \hat{s} , leaving the eigenenergies of the Hamiltonian invariant. However, the spin-conserving and spin-flip parts separately depend on the choice of the SQA.

The time-reversal and space-inversion symmetries imply that the eigenenergies of the system at any Bloch momentum \mathbf{k} are at least two-fold degenerate, with the corresponding states taking the form [2]

$$\begin{aligned} \Psi_{\mathbf{k}\hat{s}}^+(\mathbf{r}) &= [a_{\mathbf{k}\hat{s}}(\mathbf{r}) |\uparrow\rangle_{\hat{s}} + b_{\mathbf{k}\hat{s}}(\mathbf{r}) |\downarrow\rangle_{\hat{s}}] e^{i\mathbf{k}\cdot\mathbf{r}}, \\ \Psi_{\mathbf{k}\hat{s}}^-(\mathbf{r}) &= [a_{-\mathbf{k}\hat{s}}^*(\mathbf{r}) |\downarrow\rangle_{\hat{s}} - b_{-\mathbf{k}\hat{s}}^*(\mathbf{r}) |\uparrow\rangle_{\hat{s}}] e^{i\mathbf{k}\cdot\mathbf{r}}. \end{aligned} \quad (2)$$

The two spin states $|\uparrow\rangle_{\hat{s}}$ and $|\downarrow\rangle_{\hat{s}}$ are eigenstates of $\mathbf{S} \cdot \hat{s}$, e.g. if $\hat{s} \parallel z$, $|\uparrow\rangle_z$ and $|\downarrow\rangle_z$ are the eigenstates of the S_z operator. The functions $a_{\mathbf{k}\hat{s}}(\mathbf{r})$ and $b_{\mathbf{k}\hat{s}}(\mathbf{r})$ exhibit the periodicity of the crystal lattice. We define $b_{\mathbf{k}\hat{s}}^2$ as the unit cell (u.c.) integral $\int_{\text{u.c.}} d^3r |b_{\mathbf{k}\hat{s}}(\mathbf{r})|^2$.

For fixed direction \hat{s} , the degenerate $\Psi_{\mathbf{k}\hat{s}}^+$ and $\Psi_{\mathbf{k}\hat{s}}^-$ states [and the corresponding $a_{\mathbf{k}\hat{s}}(\mathbf{r})$ and $b_{\mathbf{k}\hat{s}}(\mathbf{r})$] can be chosen, by linear combination, such that the spin-expectation value $\langle S_{\hat{s}} \rangle_{\mathbf{k}} = \langle \Psi_{\mathbf{k}\hat{s}}^+ | S_{\hat{s}} | \Psi_{\mathbf{k}\hat{s}}^+ \rangle$ is maximal. The spin mixing parameter is then given by $b_{\mathbf{k}\hat{s}}^2 = 1/2 - \langle S_{\hat{s}} \rangle_{\mathbf{k}} / \hbar$, and is usually small, due to the weakness of the SOC. In this case the Bloch states are of nearly pure spin character. However, at special ‘‘spin-flip hot spot’’ points in the Brillouin zone (BZ), e.g. accidental degeneracies, BZ boundaries or other high symmetry points [11, 12], $b_{\mathbf{k}\hat{s}}^2$ may increase significantly up to $\frac{1}{2}$, which corresponds to the case of fully spin-mixed states. The Fermi-surface (FS) averaged spin-mixing, or Elliott-Yafet, parameter is given by

$$b_{\hat{s}}^2 = \frac{1}{n(E_F)} \frac{1}{\hbar} \int_{\text{FS}} \frac{b_{\mathbf{k}\hat{s}}^2}{|\mathbf{v}(\mathbf{k})|} d^2k, \quad (4)$$

where $\mathbf{v}(\mathbf{k})$ is the Fermi velocity. The normalization by the density of states at the Fermi level, $n(E_F) = 1/\hbar \int_{\text{FS}} |\mathbf{v}(\mathbf{k})|^{-1} d^2k$, ensures that $0 \leq b_{\hat{s}}^2 \leq \frac{1}{2}$.

We use density functional theory in the local density approximation [13] to calculate the electronic structure of metals considered in the following. For the self-consistent calculations we employ the Korringa-Kohn-Rostoker (KKR) Green-function method [14] in the atomic sphere approximation and solve the Dirac equation with an angular-momentum expansion up to $\ell_{\text{max}} = 4$. We choose a grid of at least 200 \mathbf{k} -points along each direction in the full Brillouin zone, resulting in about 10^7 Fermi-surface points. We follow the procedure described in Ref. [15] to maximize the spin component $S_{\mathbf{k}\hat{s}}$ at the Fermi-surface points. The details of determination of the Fermi surface and corresponding Fermi surface integration will be published elsewhere.

First, we turn to hcp osmium, which exhibits a uniaxial crystal structure, and discuss the results in detail. The Fermi surface of Os presented in Fig. 1(a-b) consists of two nested sheets, a surrounding surface crossing the BZ boundary and little hole pockets ‘‘P’’. Analyzing the distribution of the spin mixing parameter $b_{\mathbf{k}\hat{s}}^2$ on the Fermi surface, we observe a strong dependence on the SQA, evident from comparing Figs. 1(a) and (b). For \hat{s} along the c -axis of the crystal [Fig. 1(a)], the spin mixing is relatively uniform ($b_{\mathbf{k}\hat{s}}^2 \approx 0.05$) for large areas of the Fermi surface, reaching larger values near the pockets. However, this picture changes drastically when \hat{s} is parallel to the ab -plane [Fig. 1(b)]. In this case, areas with full spin mixing (red, $b_{\mathbf{k}\hat{s}}^2 \approx 0.5$) are prominent, most clearly visible at the caps of the two nested Fermi-surface sheets (indicated by ‘‘H’’). Additionally, large areas with smaller, but still strong spin mixing ($b_{\mathbf{k}\hat{s}}^2 \approx 0.3$) are visible, e.g. in the area denoted by ‘‘B’’. Overall, for the two considered cases there is a strong qualitative difference in the \mathbf{k} -dependent spin-mixing parameter $b_{\mathbf{k}\hat{s}}^2$.

As for the Fermi-surface averaged $b_{\hat{s}}^2$, we find values of 4.85×10^{-2} and 7.69×10^{-2} for \hat{s} along the c -axis and parallel to the ab -plane, respectively, yielding thus a gigantic anisotropy of the Elliott-Yafet parameter, defined as $\mathcal{A} = [\max_{\hat{s}}(b_{\hat{s}}^2) - \min_{\hat{s}}(b_{\hat{s}}^2)] / \min_{\hat{s}}(b_{\hat{s}}^2)$, of 59%. The anisotropy with respect to rotations of the SQA within the ab -plane is, on the other hand, negligible. These two limiting cases are contained in Fig. 1(g), in which the value of $b_{\hat{s}}^2$ is shown as a function of all possible directions of \hat{s} on the unit sphere. The absent (or very small) anisotropy within the ab -plane is reflected in the rotationally invariant color-scale around the c -axis, as opposed to the large difference between the ab -plane and the c -axis. A detailed analysis reveals that the largest contribution to \mathcal{A} comes from the somewhat extended areas with high or intermediate values of $b_{\mathbf{k}\hat{s}}^2$ between 0.15 and 0.35, which we refer to as ‘‘spin-flip hot areas’’ in the following.

We delve into the anisotropy of the spin-mixing at the area around H by means of a numerical experiment. Analyzing the band structure of Os along the high symmetry line from the center of the BZ (Γ -point) through the H-point to the center of the hexagonal face (A -point), in Fig. 1(e), we see two bands crossing the Fermi level at H (full black lines), representing the two nested Fermi-surface sheets of Fig. 1(a-b). The splitting Δ_{SOC} between these two bands is due to SOC, as we have

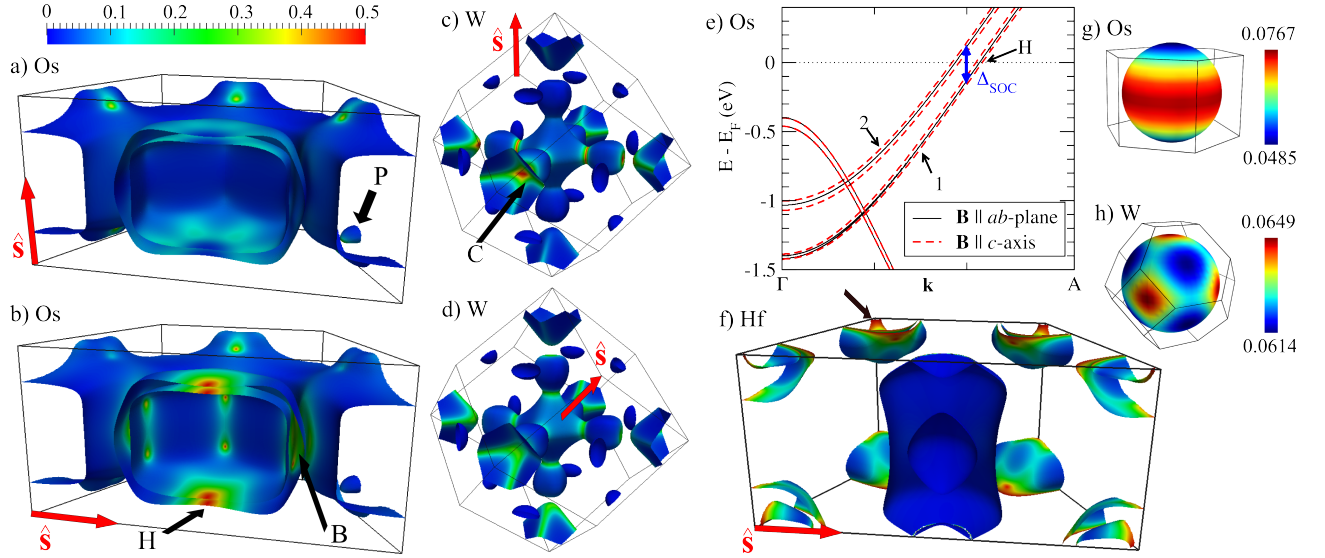


FIG. 1: (color online) Fermi surfaces of Os (a-b), W (c-d) and Hf (f). For an illustration of the nested sheets of Os and Hf, only half of the Fermi surface is shown. The Elliott-Yafet parameter $b_{\mathbf{k}\hat{\mathbf{s}}}^2$ of Os is shown in terms of a color code on the Fermi surface with the SQA $\hat{\mathbf{s}}$ [red arrows at the left-lower corners] along the c -axis (a) and in the ab -plane (b). The splitting introduced by spin-orbit coupling and by a Zeemann-like field is shown in the band structure of Os (e) along the Γ - A direction (BZ center to hexagonal-face center). Analogously, $b_{\mathbf{k}\hat{\mathbf{s}}}^2$ for $\hat{\mathbf{s}}$ along $[001]$ and $[111]$ in W is shown in (c) and (d), respectively. In (g) and (h), the integrated Elliott-Yafet parameter $b_{\hat{\mathbf{s}}}^2$ is shown as function of the SQA direction for Os and W, respectively (notice that in (g,h) the color-scale is different than in the Fermi-surface plots). The averaged values of $b_{\hat{\mathbf{s}}}^2$ over all directions of $\hat{\mathbf{s}}$, corresponding to polycrystalline samples, are 0.0666 for Os and 0.0627 for W. (f) Fermi surface of Hf with the value of $b_{\mathbf{k}\hat{\mathbf{s}}}^2$ shown as colorcode, where $\hat{\mathbf{s}}$ is parallel to the ab -plane. An arrow indicates one of the spin-flip hot loops, clearly visible in red on the hexagonal face of the BZ. The hot loops vanish when $\hat{\mathbf{s}}$ is rotated to the c -axis, resulting in an anisotropy of 830% of the Elliott-Yafet parameter.

verified by the fact that they fall on top of each other when the spin-orbit coupling strength is scaled down (not shown). Each band is twofold degenerate due to time-reversal and inversion symmetry. This remanent degeneracy can be lifted by applying a small Zeeman-like field \mathbf{B} coupling to the Bloch states via a term $\sigma \cdot \mathbf{B}$, which breaks the time-reversal symmetry and sets the SQA in the direction of \mathbf{B} . We choose a weak \mathbf{B} -field with a magnitude of 40 meV and vary its direction. In Fig. 1(e) we clearly observe a splitting of bands “1” and “2” for \mathbf{B} along the c -axis (dashed red lines). However, for \mathbf{B} in the ab -plane, the degenerate pairs “1” and “2” do not split (solid black lines). We can relate this result to our findings for $b_{\mathbf{k}\hat{\mathbf{s}}}^2$ by employing perturbation theory arguments: in first order, the energy shift of a state in presence of a small \mathbf{B} -field is proportional to the state’s spin polarization. This numerical experiment shows that in the case that $\mathbf{B} \parallel ab$ -plane the states are fully spin mixed, just as found by the calculation of $b_{\mathbf{k}\hat{\mathbf{s}}\parallel ab}^2$. It also reveals an anisotropy of the susceptibility that follows from the anisotropy of the spin-mixing parameter.

We are now in a position to give a simple line of arguments demonstrating the microscopic mechanism that leads to a large anisotropy in general. As a working example we use the calculated giant anisotropy at and in the vicinity of the H-point in Os. Important in the setup is the presence of a degeneracy or near-degeneracy at E_F , here at the point H, of Bloch wavefunctions $\Psi_{\mathbf{k}}^{1,2}$, which in a tight-binding picture we represent as $\Psi_{\mathbf{k}}^{1,2} = \sum_{lm} c_{\mathbf{k}lm}^{1,2} |l, m\rangle$. Here, $|l, m\rangle$ are eigenstates

of $\mathbf{L}_{\hat{\mathbf{s}}}$ for a given SQA $\hat{\mathbf{s}}$ in the crystal, e.g. the z axis. The requirement for a large anisotropy is met if the matrix elements of the spin-flip SOC operator $\xi(LS)^{\uparrow\downarrow}$ between $\Psi_{\mathbf{k}}^1$ and $\Psi_{\mathbf{k}}^2$ vanish. This occurs if the expansions above *exclude* terms with $l_1 = l_2$ and $|m_1 - m_2| = 1$, where $|l_1, m_1\rangle$ contributes to $\Psi_{\mathbf{k}}^1$ and $|l_2, m_2\rangle$ to $\Psi_{\mathbf{k}}^2$. Here, concretely, we have found that only the orbitals $|d, -1\rangle$ and $|d, +1\rangle$ contribute to the bands 1 and 2 at H. These are superimposed to form the oriented orbitals d_{xz} and d_{yz} which are the actual eigenstates of the crystal field. Then the lifting of degeneracy is only due to the spin-conserving SOC, $\xi(LS)_{\parallel}$ which causes no spin-mixing.

Suppose now that the SQA (and together with it the axis for quantization of orbital angular momentum) is rotated around y , from z to $\bar{z} = x$. In the new frame $(\bar{x}\bar{y}\bar{z})$ we denote the orbital functions and angular momentum indices with an overline. The oriented orbitals have a new resolution with respect to the new axes. For example, d_{yz} becomes $d_{\bar{x}\bar{y}}$ having a projection on $|\bar{d}, \pm 2\rangle$, while d_{xz} becomes $d_{\bar{x}\bar{z}}$ having a projection on $|\bar{d}, \pm 1\rangle$. As a result, the expansions of $\Psi_{\mathbf{k}}^{1,2}$ with respect to the new frame *include* orbitals with $l_1 = l_2$ and $|\bar{m}_1 - \bar{m}_2| = 1$ at the same energy, allowing for non-zero matrix elements of the spin-flip part of the SOC. For the SQA along z , the system is “protected” against large-amplitude spin-flip transitions, while for the SQA along x or y spin-flip transitions are favored. What we have demonstrated here is that the matrix elements of the spin conserving and spin-flip part of the SOC can depend so strongly on the SQA that the spin-flip vanishes

in one direction while it is maximal in another. For example, while in the original frame the SOC-induced band splitting at H arises from $\xi(LS)_{\parallel}$, in the new frame the exact same splitting arises from $\xi(LS)^{\uparrow\downarrow}$, leading to a spin mixing of $\frac{1}{2}$. It is, therefore, the direction of the SQA that dictates which part of the Hamiltonian causes most of the splitting, even though the sum of the two contributions is independent of the direction of the SQA. Other states, being higher or lower in energy due to the crystal field splitting, play only a small role in the final result.

The mechanism for large anisotropy of the spin-mixing parameter described above is of course not only specific to the d states of Os, but it is also responsible for large values of \mathcal{A} that we find for hcp Lu (200%), hcp Re (88%) and hcp Hf (830%). Particularly in hcp metals there is a special symmetry at the hexagonal face of the Brillouin zone that is lifted only by the SOC [16]. Thus, whenever the Fermi surface of an hcp metal happens to cut through the hexagonal face, the resulting contour can obtain full spin-mixing depending on the SQA, as shown in Fig. 1(f) for Hf. These looplike contours, or “spin-flip hot loops,” are a source of extremely high anisotropy. The Fermi surfaces of Lu, Re and Hf for example contain such loops, but the one of Os does not, since it does not cut through the hexagonal face.

We further observe that the magnitude of the effect can be strongly enhanced by the large extension of the two near-degenerate, parallel sheets of the Fermi surface, resulting in a spin-flip hot area around the point of near degeneracy. E.g. in Os we obtain a hot area around point H instead of a single hot spot at H, while the position and topology of such area generally depends on the Fermi surface and electronic structure of the transition metal. In addition, the reduced symmetry helps: if the crystal had cubic symmetry, then upon change of the SQA from z to x the effects at rotationally equivalent parts of the Fermi surface would mutually cancel.

We now turn to tungsten, which has a bcc lattice structure. When $\hat{s} \parallel [001]$, $b_{\mathbf{k}\hat{s}}^2$ exhibits hot spots in directions perpendicular to \hat{s} (denoted by “C”) [Fig. 1(c)], but not at the rotationally equivalent points along the z -axis, following the formation scenario similar to that at the H-point in Os. Additionally, many states with smaller spin mixing ($0.2 < b_{\mathbf{k}\hat{s}}^2 < 0.3$) are present at the Fermi surface, leading to $b_{\hat{s}}^2 = 6.49 \times 10^{-2}$. For SQA along another high symmetry direction of the lattice, $\hat{s} \parallel [111]$ in Fig. 1(d), the intensity at the point C is reduced, but a large area with smaller spin mixing is clearly present, resulting in $b_{\hat{s}}^2 = 6.14 \times 10^{-2}$. For SQA along $[110]$, we find $b_{\hat{s}}^2 = 6.26 \times 10^{-2}$. This leads to an anisotropy $\mathcal{A} = 6\%$, which is still large but one order of magnitude smaller than in hcp Os. In fact we also predict rather small anisotropy in other cubic transition metals, such as Ir (1%) and Pt (0.4%). This observation is similar to the dependence of the magnetocrystalline anisotropy energy and anisotropy of the intrinsic anomalous Hall conductivity [17, 18] on the symmetry of the lattice in ferromagnetic crystals: the cubic crystal exhibits a fourfold rotational axis, causing SOC to contribute to \mathcal{A} in fourth order. In the uniaxial hcp structure, an axis perpendic-

ular to the c -axis is only twofold, leading SOC to enter \mathcal{A} in second order. Generally we expect the integrated value $b_{\hat{s}}^2$ to exhibit the full point-group symmetry of the lattice (evident in Fig. 1(g) for Os and (h) for W), even if the map of $b_{\mathbf{k}\hat{s}}^2$ has a lower symmetry. The comparatively large anisotropy value in W is partly a consequence of the d -states, which yield a strong directional anisotropy of the Fermi surface. In contrast to this, the Fermi surface of fcc gold consists of s -like states and can be regarded as almost spherical. For the Elliott-Yafet parameter in Au, we find $b_{\hat{s}}^2 \approx 3.25 \times 10^{-2}$, i.e. the same order of magnitude as in W and Os, but the anisotropy is only 0.1%.

A measurement of the anisotropy requires samples with preferential crystalline orientation and a rotation of the magnetic field direction in an electron spin resonance experiment or a rotation of the magnetization direction of the ferromagnetic injector in a spin-injection experiment. In reality, the precise scattering mechanism will naturally affect the result. Nevertheless our results should be plainly measurable even if the exact value can deviate somewhat from the one of the Elliott approximation. Perhaps the anisotropy, stemming from the band structure, can be most conveniently measured as a function of the temperature invoking phonon scattering, in order to circumvent any possible extrinsic anisotropy arising from the electronic structure of defects in the system.

In conclusion, spin relaxation in metals can strongly depend on the orientation of the injected-electron spin axis due to a corresponding anisotropy of the Elliott-Yafet parameter. The anisotropy is expected to be largest in non-cubic crystals and in the presence of extended nested Fermi-surface sheets that are almost degenerate, resulting in extended spin hot areas or hot loops instead of singular spin hot spots; especially critical are cases where the splitting between nested sheets is caused primarily by the spin-orbit coupling. Since there is no theoretical limit on the area of the nested sheets in this scenario, the anisotropy can in principle exceed the large values calculated here and is an effect worthwhile investigating on a number of metals and ordered alloys. Possible symmetry reduction by the Fermi-surface nesting, e.g. charge-density waves, would be of long wavelength because of the smallness of the \mathbf{k} -vector connecting the split Fermi-surface sheets, therefore we expect a small reduction but not a fundamental change by such effects. Temperature or moderate alloying can blur out the sharpness of the bands, but if the band splitting is on the order of 0.2–0.3 eV (approx. 2000–3000 Kelvin), and the bandwidth of the critical bands on the order of 1–2 eV, as we found in the case of Os, then the blurring of the bands will not be sufficient to mask the anisotropy. We furthermore expect that anisotropy effects should also be present in metallic alloys, heterostructures or ultrathin films, which we leave for future work.

We are indebted to J. Fabian for an introduction to the field and for discussions. We are also indebted to R. Zeller and P. H. Dederichs for their invaluable help in the KKR formalism and to G. Bihlmayer, D.V. Fedorov and P. Zahn for discussions. We acknowledge funding under project MO 1731/3-1 and the Priority Programme SPP-1538 “Spin Caloric

Transport” of the Deutsche Forschungsgemeinschaft, the Helmholtz-Gemeinschaft Young Investigators programme VH-NG-513, as well as computing time at the Jülich Supercomputing Centre.

* Electronic address: Ph.Mavropoulos@fz-juelich.de

- [1] I. Žutić, J. Fabian, and S. Das Sarma, *Rev. Mod. Phys.* **76**, 323 (2004).
- [2] R. J. Elliott, *Phys. Rev.* **96**, 266 (1954).
- [3] Y. Yafet, in: *Solid State Physics* (Eds. F. Seitz and D. Turnbull) **14**, 1 (1963).
- [4] An anisotropy of spin relaxation has been measured in supported graphene layers [5] and discussed for semiconductors [6]; however, these are systems without space inversion symmetry where the Dyakonov-Perel mechanism is likely dominant.
- [5] N. Tombros, S. Tanabe, A. Veligura, C. Jozsa, M. Popinciuc, H. T. Jonkman, and B. J. van Wees, *Phys. Rev. Lett.* **101**, 046601 (2008).
- [6] N. S. Averkiev and L. E. Golub, *Semiconductor Science and Technology* **23**, 114002 (2008).
- [7] H. Katayama-Yoshida, T. Fukushima, V. An Dinh, and K. Sato, *Jpn. J. Appl. Phys.* **46**, L777 (2007); A. Sugihara, M. Kodzuka, K. Yakushiji, H. Kubota, S. Yuasa, A. Yamamoto, K. Ando, K. Takanashi, T. Ohkubo, and K. Hono, *Appl. Phys. Express* **3**, 065204 (2010).
- [8] F. Freimuth, S. Blügel, and Y. Mokrousov, *Phys. Rev. Lett.* **105**, 246602 (2010).
- [9] M. Gradhand, M. Czerner, D. V. Fedorov, P. Zahn, B. Y. Yavorsky, L. Szunyogh, and I. Mertig, *Phys. Rev. B* **80**, 224413 (2009).
- [10] D. Steiauf and M. Fähnle, *Phys. Rev. B* **79**, 140401 (2009); K. Carva, M. Battiato, and P. M. Oppeneer, *Phys. Rev. Lett.* **107**, 207201 (2011).
- [11] J. Fabian and S. Das Sarma, *Phys. Rev. Lett.* **81**, 5624 (1998).
- [12] J. Fabian and S. Das Sarma, *Phys. Rev. Lett.* **83**, 1211 (1999).
- [13] S. H. Vosko, L. Wilk, and M. Nusair, *Can. J. Phys.* **58**, 1200 (1980).
- [14] H. Ebert and R. Zeller, *The SPR-TB-KKR package*, URL <http://olymp.cup.uni-muenchen.de/ak/ebert/SPR-TB-KKR>.
- [15] S. Heers, Ph.D. thesis, RWTH Aachen (2011). URL <http://darwin.bth.rwth-aachen.de/opus3/volltexte/2011/3827>.
- [16] N. W. Ashcroft and D. N. Mermin, *Solid State Physics*, Saunders College Publishing (1976), p.299.
- [17] C. Zener, *Phys. Rev.* **96**, 1335 (1954).
- [18] E. Roman, Y. Mokrousov, and I. Souza, *Phys. Rev. Lett.* **103**, 097203 (2009).